Correlating structure and detection properties in HgTe nanocrystal films

Correlating Structure and Detection Properties in HgTe Nanocrystal Films

Sang-Soo Chee[1,2], Charlie Gréboval[1], Debora Vale Magalhaes[3,4], Julien Ramade[3,4], Audrey Chu[1], Junling Qu[1], Prachi Rastogi[1], Adrien Khalili[1], Tung Huu Dang[1,5], Corentin Dabard[1], Yoann Prado[1], Gilles Patriarche[6], Julien Chaste[6], Michael Rosticher[5], Sara Bals[3,4], Christophe Delerue[7], Emmanuel Lhuillier[1*]

[1] Sorbonne Université, CNRS, Institut des NanoSciences de Paris, 4 place Jussieu, 75005 Paris, France.
[2] Nanomaterials and Nanotechnology Center, Korea Institute of Ceramic Engineering and Technology (KICET), 101 Soho-ro, 52851 Jinju-si, Republic of Korea
[3] Electron Microscopy for Materials Science, University of Antwerp, Groenenborgerlaan 171, B-2020 Antwerp, Belgium.
[4] NANOlab Center of Excellence, University of Antwerp, Belgium
[5] Laboratoire de Physique de l'Ecole normale supérieure, ENS, Université PSL, CNRS, Sorbonne Université, Université Paris-Diderot, Sorbonne Paris Cité, Paris, France Paris.
[6] Centre de Nanosciences et de Nanotechnologies, CNRS, Université Paris-Saclay, C2N, Palaiseau 2110, France.
[7] Univ. Lille, CNRS, Centrale Lille, Univ. Polytechnique Hauts-de-France, Junia, UMR 8520 - IEMN, F-59000 Lille, France

Abstract: HgTe nanocrystals (NCs) enable broadly tunable infrared absorption, now commonly used to design light sensors. This material tends to grow under multipodic shapes and does not present well-defined size distributions. Such point generates traps and reduces the particle packing leading to a reduced mobility. It is thus highly desirable to comprehensively explore the effect of the shape on their performance. Here, we show, using a combination of electron tomography and tight binding simulations, that the charge dissociation is strong within HgTe NCs, but poorly shape dependent. Then, we design a dual-gate field-effect-transistor made of tripod HgTe NCs and use it to generate a planar *p*-*n* junction, offering more tunability than its vertical geometry counterpart. Interestingly, the performance of the tripods is higher than sphere ones, and this can be correlated with a stronger Te excess in the case of sphere shapes which is responsible for a higher hole trap density.

Keywords: HgTe, electron tomography, tight binding simulation, *p*-*n* junction, field-effect transistor, gate effect.

* To whom correspondence should be sent: el@insp.upmc.fr

II-VI semiconductors are the most mature materials under colloidal quantum dot (CQD) form and have been extensively used for optoelectronic applications. Among them, HgTe is certainly offering the widest spectral tunability and the most impressive device performance for infrared light emission[1–3] and detection.[4–6] Over the recent years, the integration of HgTe CQDs as absorbing layers in IR sensors has been developed from the basic demonstration of IR photoconduction,[7,8] to highly complex devices including focal plane arrays[9–13] and unconventional detectors with enhanced light-matter coupling to increase their light absorption.[14–18] A significant part of the efforts has been dedicated to improve the device, including the development of vertical geometry devices (*i.e.* photodiodes) thanks to the development of hole extracting layers[19] and unipolar barriers[20,21] suitable for narrow band-gap materials. In addition, planar geometry devices (*i.e.* phototransistors)[18,22,23], enable to efficiently control the carrier density by applying a gate bias, which maximizes the signal to noise ratio.

As the field gains maturity, the material itself may become a limitation. The decrease of the non-radiative recombination rates[24] has been identified as a key element to reduce the noise in detectors. The surface chemistry, through the control of traps and surface dangling bonds, plays a major role in the decrease of this non-radiative processes. However, this is not the only source of traps. Size polydispersity, via quantum confinement, induces that the largest particles behave as traps. In the case of HgTe, the material synthesis has been focused on increasing the material size to push the absorption and emission toward longer wavelengths. It is worth pointing that most syntheses (either based on aqueous or organic paths) lead to non-spherical shape particles such as multipods[25,26]. The uncertain shape definition results in a clear broadening of the size distribution and finally generates traps. Such traps might offer beneficial roles such as the formation of a three-level systems for low threshold lasing[2] or the demonstration of memory effect.[27] In HgTe CQDs, it can also lead to poor transport properties with lower transport activation energies, which reduces performance increase upon cooling.[28] Beyond the formation of traps, the growth of multipodic shape particles may also induce a poor particle packing within the film, resulting in a distribution of particle distances which consequently limits the film mobility and generates noise[29]. Only recently, the growth of quasi spherical HgTe CQDs have been achieved[30,31] which has reduced the size distribution and has finally lead to improved film mobilities higher than 1 $cm^2V^{-1}s^{-1}$.[29,30] However, their spectra are broader than the ones obtained from multipodic HgTe, in spite of a better size control.[34] It is thus of utmost interest to reveal how the shape is linked to the performance obtained so far for IR detection.

In this paper, we investigate how the structural and electronic properties of HgTe nanocrystals are connected to each other and how they impact the device performance. To reach this goal, we use a two scales approach. First, at the single particle level, we combine electron tomography and tight binding simulations to reveal the wavefunctions and their overlap for realistic particle shapes. Then, in a second step, we integrate the grown material into a dual gate field-effect transistor (FET), enabling us to design, on-demand carrier density profiles. While this strategy is widely used in the field of 2D materials and mesoscopic physics[35–40], it has not been applied yet to CQD-based devices. The dual gate FET enables the design of planar tunable *p-n* junctions from which we can estimate the influence of the local morphology, including the trap distribution, and electronic structure, on the charge dissociation at a mesoscopic scale.

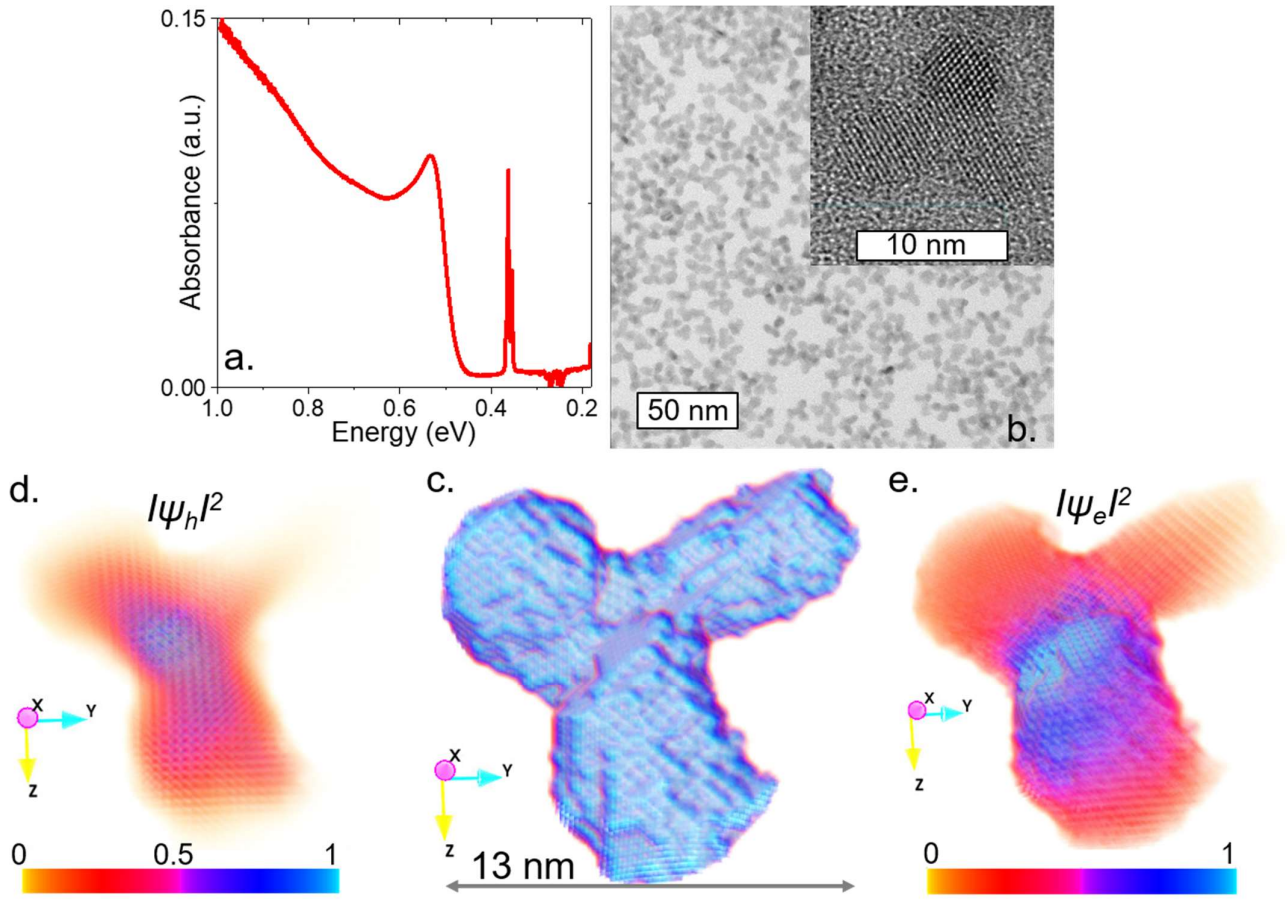

***Figure 1**. a. Infrared absorption spectrum of HgTe CQDs with a 4000 cm^{-1} (or ≈0.5 eV, HgTe 4k) band-edge energy. b. Transmission electron microscopy image of those HgTe 4k CQDs. The inset is a high resolution image of a single CQD. c. Reconstruted morphology of a HgTe CQD as revealed from electron tomography. d. (resp. e.) Square modulus of the 3D hole (resp. electron) wavefunction for a HgTe tripod revealed from tomography.*

We synthesize HgTe CQDs following the procedure by Keuleyan *et al.*[26] The obtained particles present absorption in the extended short-wave IR (SWIR) with a cut-off wavelength at 2.5 µm (4000 cm^{-1} or ≈500 meV), see **Figure 1**a and S1-S4. Electron microscopy clearly reveals the branched shape of the obtained CQDs (see **Figure 1**b and its high-resolution inset image). To further reveal the actual CQD shape, we use electron tomography to obtain a 3D reconstruction of the particle, see **Figure 1**c, Figure S5, S8 and video S1. While from TEM the particle shape has for long been inferred to be a tetrapod,[26] it appears that the actual shape is more in agreement with a tripod.

This measured shape is then used as an input for atomistic tight-binding simulations of the electronic structure. The absorption spectrum is calculated using the Fermi Golden rule[41–43], see Figure S6. Due to the strong mass asymmetry in HgTe[44] (a hole is about 25 times heavier than an electron), the hole wavefunction is more localized in the center and its presence at the edge of the tripod arms is weaker compared to the electron, see **Figure 1**d-e and S7-S10. From these wavefunctions, we can quantify the wavefunction overlap (see table S1) which is directly linked to the binding energy of the electron-hole pair. The overlap appears to be weak around 0.4, but poorly dependent on the particle shape. In HgTe, due to the strong effective mass asymmetry, the electron is strongly confined and its wavefunction explore the whole structure while the hole with its large mass stay located in the center of the structure. This contrasts with materials such as PbS where the electron and hole effective masses are identical. In this sense, the electronic structure of HgTe favors electron-hole dissociation in nanostructures, while the shape plays no role in the charge dissociation.

Since the particle shape is barely impacting the HgTe CQD quantum state overlap, we further explore how particle geometry affects the photocurrent. We demonstrated that the charge dissociation is independent of the particle shape, but it may still have an effect through trap distribution, film packing, *etc*... Vertical geometry

photodiode is certainly the most effective strategy to achieve detection with high signal to noise ratio, but it suffers from a lack of post-fabrication tunability to determine improvement strategies. By contrast, phototransistors[22] can offer more flexibility thanks to an efficient tunability of the carrier density in the channel by applying gate bias. Here, we use a planar dual gate FET to explore the effects of doping and particle geometry for detection. From a pure detection point of view, vertical geometry enables a better charge extraction since the device size is reduced down to the short carrier diffusion length resulting from hopping mechanism. However, our strategy due to its tunability, is used to reveal the origin of the observed low V_{OC} in current HgTe photodiodes.

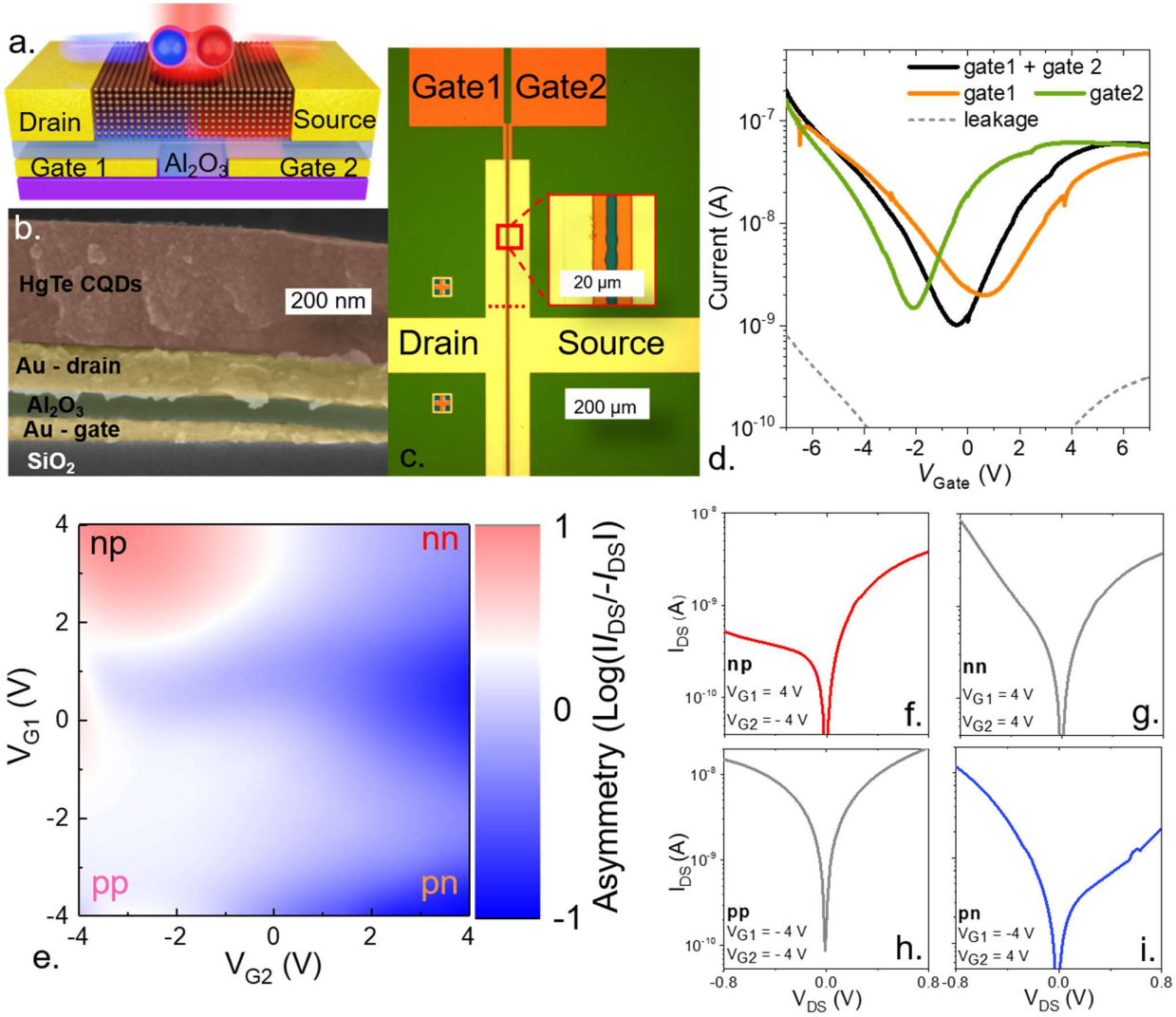

Figure 2 *a. Sketch of the dual gate device inducing charge dissociation. b. Cross section, along horinzontal red dashed line according to image in part c, of the device using scanning electron microscopy. c. Top view of the device acquired from optical microscopy. d. Transfer curves (drain and gate currents as a function of the applied gate bias while the drain source bias is set to 1 V) while gate 1, gate 2 (with the other gate is floating), or gate 1 + gate 2 are tuned. e. Map of the I-V curve asymetry (defined here as the log of the ratio of the current under +0.5 V and -0.5 V) as a function of the applied biases of gate 1 and gate 2. f-i are respectively the I-V curves in the n-p, n-n, p-p, and p-n. All measurements are conducted at 250 K.*

The gates from the FET device need to match two strong requirements: first, (*i*) it has to enable a large carrier density modulation (*i.e.* presents a large capacitance) to generate a large in-built electric field. Second, (*ii*) it needs to be compatible with microfabrication methods to design a p-i-n junction where the intrinsic zone size remains close to the ones used in vertical geometry devices (*i.e.* the distance between the two gates should be similar to the thickness of a photodiode ≈500 nm). While various high capacitance gating strategies have been explored recently for HgTe CQD films including electrolyte,[45,46] ionic glasses,[23,47] and ferroelectric[18] materials, none of these methods appear to be convenient to spatially define the gate. This is why we chose

a more conventional approach based on Al_2O_3 grown using atomic layer deposition (ALD) as a high-k material. The design of the device is given in **Figure 2**a-c and S11-12.

We first confirm that both gates can be used with low leakage current, see **Figure 2**d and S13. Current modulation is typically a factor around 100 at 250 K and shows a clear ambipolar behavior with both hole and electron conductions. In the next step, we test the potential of the gates to induce non Ohmic I-V curves. We quantify the rectifying behavior of the I-V curves through the ratio of current $I(V_{DS})/I(-V_{DS})$, see **Figure 2**e. We clearly observe that, under conditions such as $V_{G1}=V_{G2}$ (for example in *n-n* and *p-p* regime on **Figure 2**e), the asymmetry ratio is small and the I-V curves show quasi-ohmic behaviors, see **Figure 2**g and h. On the other hand, under gate biases such as $V_{G1}=-V_{G2}$ (*p-n* and *n-p* regime), I-V curves get rectified (**Figure 2**f and i) and the curve asymmetry is maximized, as expected for a *p-n* junction.

We then investigate the potential of the dual gate device for charge dissociation. In the phototransistor regime (*n-n* or *p-p* part of the phase diagram), not any open-circuit voltage (V_{OC}) is generated under the sample illumination, see **Figure 3**a and b. On the other hand, in the diode regime (*p-n* or *n-p* in the phase diagram), V_{OC} are clearly observed. Those V_{OC} can reach 180 mV under 1 $W.cm^{-2}$ at 1.55 µm (**Figure 3**c), corresponding to 36% of the optical band gap value. The V_{OC} of the dual gate device presents a linear temperature dependence of 770 $\mu V.K^{-1}$ (see Figure S15), implying that the 180 mV value measured at 250 K can be extrapolated to a V_{OC} of 214 mV at room temperature (42 % of the band-gap). To obtain such V_{OC} values using a vertical geometry diode (ITO/HgTe/Ag_2Te/gold structure[48]), the band-gap of HgTe has to be increased by 50% (reaching now 800 meV, corresponding to HgTe CQDs with band edge at 6000 cm^{-1}), see Figure S19. Part of the discrepancy might be due to a lower performing diode. Nevertheless, particularly under low photon flux, V_{OC} stays much higher in the dual-gate device due to an optimized carrier density profile.

V_{OC} appears to be robust to the geometrical factor of the device. As the film thickness is reduced from 200 nm to 50 nm, only a small drop (≈20 mV, which is in the range of the V_{OC} fluctuations observed from device to device) of the V_{OC} is observed (Figure S14). It is also worth pointing out that such V_{OC} are obtained with a gate separation of 3 µm, which is wider than the thickness of a typical diode. This means that the screening of the *p*- and *n*-doped regions is weak due to the limited dielectric constant of a nanocrystal film in presence of organic ligands ($\varepsilon_r<8$). The reduced dielectric constant compared to the bulk (or PbS NCs) is certainly responsible for the possibility to gate thick films of HgTe CQDs even using a back gating approach. It also suggests that future designs of HgTe CQD-based diodes can afford the presence of thick intrinsic absorbing layers between the *p* and *n* doped layers, used to extract electrons and holes, without any reduction of the V_{OC}.

While the V_{OC} seems to be robust toward the geometrical factor, it appears to be dramatically impacted by the size and shape distributions. To address this question, we intentionally prepare a polydisperse HgTe CQD solution by mixing two batches of nanocrystals (Figure S20-21), while keeping the average cut-off wavelength unchanged. In such mixture, the large CQDs are expected to behave as trap states, generating states within the band gap of the smallest and more confined ones. This procedure should affect the V_{OC}[49] as it is commonly observed for PbS CQD-based solar cells.[50] HgTe CQDs, thanks to their non-dispersive valence band,[51] have been identified to be more robust to polydispersity than intraband materials such as HgSe. However, a broad size distribution impacts the transport through a reduction of the current modulation obtained in the FET configuration (Figure S21). As expected, the V_{OC} is also reduced, see **Figure 3**c. Using this polydisperse material, the V_{OC} barely reaches 60 mV. This corresponds to a third of the value measured from the material with better size distribution.

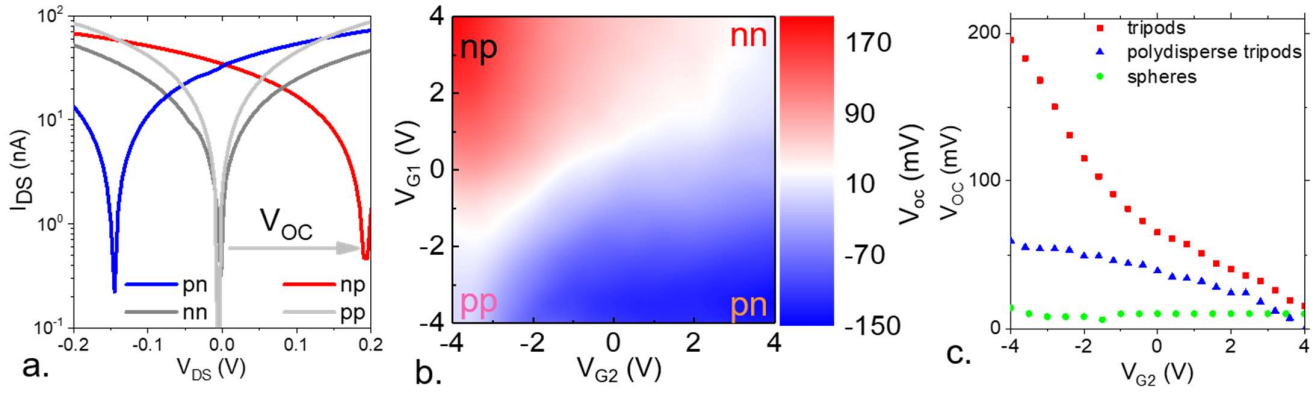

Figure 3 *a. I-V curves under illumination (@1.55 µm - 1W.cm^{-2}) while the device is operated in the n-p, n-n, p-p, and p-n regimes. b. Open circuit voltage (V_{OC}) map as a function of applied gate 1 and gate 2 biases. c. V_{OC} as a function of applied bias on gate 2, while the bias on gate 1 is set equal to +4 V for three population of HgTe nanocrystals : monodisperse tripods, polydisperse tripods and round particles. All data are measured at 250 K.*

We have also tested spherical HgTe CQDs (**Figure 3**c and S22-25) and found an even lower V_{OC} (≈25 mV). This may explain why, to date, the use of spherical shaped HgTe CQDs for diodes remains unreported. This result highlights that monodispersity is not sufficient to obtain highly performing devices[52,53] and that the optimal surface chemistry clearly depends on the particle shape. To confirm this hypothesis, we have performed Energy Dispersive X-ray spectroscopy (EDX) coupled to TEM (figure S3 and S4 for tripods and S23-24 for quasi spheres of HgTe. While many previous reports[54] based on EDX coupled with scanning electron microscopy (SEM) have claimed for quasi stoichiometric particles, EDX coupled to TEM reveals a clear Te excess (55% Te atomic ratio in the case of tripods) that is even stronger in the case of quasi sphere-shaped HgTe (63% Te atomic ratio). Such Te excess is known to generate hole traps.[2] We then quantize the impact of the traps through transport (Figure S25). At room temperature, fast release from traps is possible and the mobility appears higher for quasi sphere-shaped CQDs thanks to their better packing (Figure S25b). At low temperature, thermal detrapping is reduced, and a higher mobility for tripods is observed (Figure S25c).

The ability of the dual-gate device for light detection is better highlighted from the responsivity map, see **Figure 4**a, S16-17. It is clear that the highest response values are obtained under gate conditions corresponding to the diode regime (V_{G1}=-V_{G2}). Under the application of a small reverse bias (V_{DS}=-0.5 V, see figure S16-17), The achieved responsivity reaches a few tens of mA.W^{-1}, which is typical for photoconductive devices operated in the hopping regime, see table S3 for a comparison of this device with state-of-the-art devices. Currently the absorption (≈10%) is limiting the device performance and a future challenge will be to couple such geometry with light resonators to bring up the absorption close to 1.

The diode regime combines enhanced photocurrent and low dark current due to 0 V operation. As a result, the current modulation under illumination at 0 V increases from 0 in the phototransistor regime (V_{GS}>0) to >10^4 for the diode operating mode (V_{GS}<0), see **Figure 4**b. Such significant improvement of the light detection properties is obtained while the time response remains fast with a turn-off time measured equal to 25 µs in the diode mode (**Figure 4**c-d). This time is barely longer than the one obtained in the phototransistor mode (5-7 µs) which is setup limited. We estimate the detectivity to range between 10^8 and 10^{10} Jones range at 250 K and for 1 kHz operation at 1.55 µm (see discussion in the SI, Figure S18 and Table S2-3).

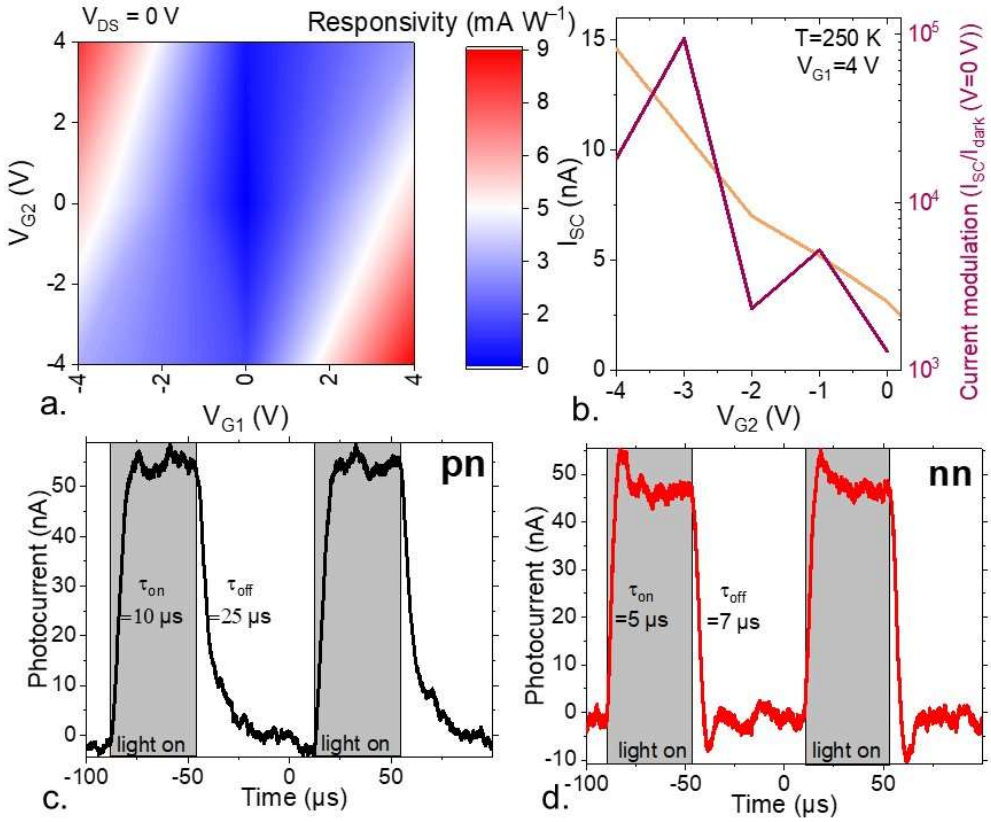

Figure 4 a. *Responsivity map under null drain source bias as a function of applied gate 1 and gate 2 biases, highlighting an enhanced photocurrent generation in the range of gate biases corresponding to the formation of p-n (or n-p) junction. b. Short circuit current and current modulation (short circuit current divided by dark current) as a function of* V_{G2} *(*V_{G1} *= +4 V is constant) under an irradiance of 1 W.cm*$^{-2}$ *at 1.55 µm. c. Current as a function of time as a laser source (1.55 µm) is turned on and off, while the gates are set to operate in the n-p regime (*V_{G1}=4 V ;V_{G2}=-4 V). *d. Current as a function of time as a laser source (1.55 µm) is turned on and off, while the gates are set to operate in the n-n regime* (V_{G1}=4 V ;V_{G2}=4 V). *For parts c and d, a small* V_{DS}*=0.5 V is applied to obtain some signal in the phototransistor configuration.*

To summarize, we have studied the correlation between the particle morphology and the device performance in HgTe CQD films used for IR sensing thanks to a combination of nanoscale (electron tomography and tight binding simulations) and mesoscale (dual gate FET) measurements. In HgTe CQDs, there is a pre-existing charge dissociation, which does not relate to the particle shape, but to the asymmetry of the effective masses. We then use the dual gate FET to generate, on demand, doping profiles and create *p-n* junctions. The obtained V_{OC} is now reaching ≈40% of the optical band gap. Operation of the device in the diode mode allows an increase in the photoinduced current modulation by more than 4 orders of magnitude, while presenting a fast time response (25 µs fall time). We show that polydispersity can dramatically impact V_{OC} of the dual gate device in the diode regime. Moreover, the use of monodisperse sphere shaped particles is not leading to a better performing device despite a higher film mobility at room temperature. Such interesting behavior is attributed to shape-dependent stoichiometry of HgTe NCs; a larger Te excess is observed in the case of spherical CQDs finally resulting in a larger hole trap density. Our findings suggest that more efforts will have to be devoted in the future to the surface healing.

ACKNOWLEDEGMENTS

The project is supported by ERC starting grant blackQD (grant n° 756225) and consolidator grant Realnano (815128). This project has received funding from the European Commission (grant 731019, EUSMI). We acknowledge the use of clean-room facilities from the “Centrale de Proximité Paris-Centre”. This work has been supported by the Region Ile-de-France in the framework of DIM Nano-K (grant dopQD). This work was supported by French state funds managed by the ANR within the Investissements d'Avenir programme under reference ANR-11-IDEX-0004-02, and more specifically within the framework of the Cluster of Excellence MATISSE and also by the grant IPER-Nano2 (ANR-18CE30-0023-01), Copin (ANR-19-CE24-0022), Frontal (ANR-19-CE09-0017), Graskop (ANR-19-CE09-0026) and NITQuantum (ANR-20-ASTR-0008-01). AC thanks Agence innovation defense for PhD funding.

SUPPORTING INFORMATION

Supporting Information include details about material synthesis and characterization, tight binding atomistic simulation, fabrication of the dual gate device, and fabrication of HgTe CQD based photodiode.

COMPETING INTEREST

The authors declare no competing financial interest.

REFERENCES

(1) Sergeev, A. A.; Pavlov, D. V.; Kuchmizhak, A. A.; Lapine, M. V.; Yiu, W. K.; Dong, Y.; Ke, N.; Juodkazis, S.; Zhao, N.; Kershaw, S. V.; et al. Tailoring Spontaneous Infrared Emission of HgTe Quantum Dots with Laser-Printed Plasmonic Arrays. *Light Sci. Appl.* **2020**, *9*, 16.

(2) Geiregat, P.; Houtepen, A. J.; Sagar, L. K.; Infante, I.; Zapata, F.; Grigel, V.; Allan, G.; Delerue, C.; Van Thourhout, D.; Hens, Z. Continuous-Wave Infrared Optical Gain and Amplified Spontaneous Emission at Ultralow Threshold by Colloidal HgTe Quantum Dots. *Nat. Mater.* **2018**, *17*, 35–42.

(3) Qu, J.; Rastogi, P.; Gréboval, C.; Lagarde, D.; Chu, A.; Dabard, C.; Khalili, A.; Cruguel, H.; Robert, C.; Xu, X. Z.; et al. Electroluminescence from HgTe Nanocrystals and Its Use for Active Imaging. *Nano Lett.* **2020**, *20*, 6185–6190.

(4) Hao, Q.; Tang, X.; Cheng, Y.; Hu, Y. Development of Flexible and Curved Infrared Detectors with HgTe Colloidal Quantum Dots. *Infrared Phys. Technol.* **2020**, *108*, 103344.

(5) Lhuillier, E.; Guyot-Sionnest, P. Recent Progresses in Mid Infrared Nanocrystal Optoelectronics. *IEEE J. Sel. Top. Quantum Electron.* **2017**, *23*, 6000208.

(6) Hafiz, S. B.; Scimeca, M.; Sahu, A.; Ko, D.-K. Colloidal Quantum Dots for Thermal Infrared Sensing and Imaging. *Nano Converg.* **2019**, *6*, 7.

(7) Böberl, M.; Kovalenko, M. V.; Gamerith, S.; List, E. J. W.; Heiss, W. Inkjet-Printed Nanocrystal Photodetectors Operating up to 3 μm Wavelengths. *Adv. Mater.* **2007**, *19*, 3574–3578.

(8) Keuleyan, S.; Lhuillier, E.; Brajuskovic, V.; Guyot-Sionnest, P. Mid-Infrared HgTe Colloidal Quantum Dot Photodetectors. *Nat. Photonics* **2011**, *5*, 489–493.

(9) Chu, A.; Martinez, B.; Ferré, S.; Noguier, V.; Gréboval, C.; Livache, C.; Qu, J.; Prado, Y.; Casaretto, N.; Goubet, N.; et al. HgTe Nanocrystals for SWIR Detection and Their Integration up to the Focal Plane Array. *ACS Appl. Mater. Interfaces* **2019**, *11*, 33116–33123.

(10) Chatterjee, A.; Pendyala, N. B.; Jagtap, A.; Rao, K. S. R. K. Uncooled Mid-Wave Infrared Focal Plane Array Using Band Gap Engineered Mercury Cadmium Telluride Quantum Dot Coated Silicon ROIC. *E-J. Surf. Sci. Nanotechnol.* **2019**, *17*, 95–100.

(11) Buurma, C.; Pimpinella, R. E.; Ciani, A. J.; Feldman, J. S.; Grein, C. H.; Guyot-Sionnest, P. MWIR Imaging with Low Cost Colloidal Quantum Dot Films. *Opt. Sens. Imaging Photon Count. Nanostructured Devices Appl. 2016* **2016**, *9933*, 993303.

(12) Gréboval, C.; Ferre, S.; Noguier, V.; Chu, A.; Qu, J.; Chee, S.-S.; Vincent, G.; Lhuillier, E. Infrared Narrow Band Gap Nanocrystals: Recent Progresses Relative to Imaging and Active Detection. 2020 *ArXiv200111554. Cond-Mat.* https://arxiv.org/abs/2001.11554 (accessed April 30th, 2021).
(13) Ciani, A. J.; Pimpinella, R. E.; Grein, C. H.; Guyot-Sionnest, P. Colloidal Quantum Dots for Low-Cost MWIR Imaging. *Infrared Technol. Appl. XLII* **2016**, *9819*, 981919.
(14) Chen, M.; Shao, L.; Kershaw, S. V.; Yu, H.; Wang, J.; Rogach, A. L.; Zhao, N. Photocurrent Enhancement of HgTe Quantum Dot Photodiodes by Plasmonic Gold Nanorod Structures. *ACS Nano* **2014**, *8*, 8208–8216.
(15) Tang, X.; Ackerman, M. M.; Guyot-Sionnest, P. Acquisition of Hyperspectral Data with Colloidal Quantum Dots. *Laser Photonics Rev.* **2019**, *13*, 1900165.
(16) Tang, X.; Ackerman, M. M.; Guyot-Sionnest, P. Thermal Imaging with Plasmon Resonance Enhanced HgTe Colloidal Quantum Dot Photovoltaic Devices. *ACS Nano* **2018**, *12*, 7362–7370.
(17) Chu, A.; Gréboval, C.; Goubet, N.; Martinez, B.; Livache, C.; Qu, J.; Rastogi, P.; Bresciani, F. A.; Prado, Y.; Suffit, S.; et al. Near Unity Absorption in Nanocrystal Based Short Wave Infrared Photodetectors Using Guided Mode Resonators. *ACS Photonics* **2019**, *6*, 2553–2561.
(18) Gréboval, C.; Chu, A.; Magalhaes, D. V.; Ramade, J.; Qu, J.; Rastogi, P.; Khalili, A.; Chee, S.-S.; Aubin, H.; Vincent, G.; et al. Ferroelectric Gating of Narrow Band-Gap Nanocrystal Arrays with Enhanced Light–Matter Coupling. *ACS Photonics* **2021**, *8*, 259–268.
(19) Ackerman, M. M.; Tang, X.; Guyot-Sionnest, P. Fast and Sensitive Colloidal Quantum Dot Mid-Wave Infrared Photodetectors. *ACS Nano* **2018**, *12*, 7264–7271.
(20) Jagtap, A.; Martinez, B.; Goubet, N.; Chu, A.; Livache, C.; Gréboval, C.; Ramade, J.; Amelot, D.; Trousset, P.; Triboulin, A.; et al. Design of a Unipolar Barrier for a Nanocrystal-Based Short-Wave Infrared Photodiode. *ACS Photonics* **2018**, *5*, 4569–4576.
(21) Gréboval, C.; Noumbé, U. N.; Chu, A.; Prado, Y.; Khalili, A.; Dabard, C.; Dang, T. H.; Colis, S.; Chaste, J.; Ouerghi, A.; et al. Gate Tunable Vertical Geometry Phototransistor Based on Infrared HgTe Nanocrystals. *Appl. Phys. Lett.* **2020**, *117*, 251104.
(22) Chen, M.; Lu, H.; Abdelazim, N. M.; Zhu, Y.; Wang, Z.; Ren, W.; Kershaw, S. V.; Rogach, A. L.; Zhao, N. Mercury Telluride Quantum Dot Based Phototransistor Enabling High-Sensitivity Room-Temperature Photodetection at 2000 nm. *ACS Nano* **2017**, *11*, 5614–5622.
(23) Gréboval, C.; Noumbe, U.; Goubet, N.; Livache, C.; Ramade, J.; Qu, J.; Chu, A.; Martinez, B.; Prado, Y.; Ithurria, S.; et al. Field-Effect Transistor and Photo-Transistor of Narrow-Band-Gap Nanocrystal Arrays Using Ionic Glasses. *Nano Lett.* **2019**, *19*, 3981–3986.
(24) Guyot-Sionnest, P.; Ackerman, M. M.; Tang, X. Colloidal Quantum Dots for Infrared Detection beyond Silicon. *J. Chem. Phys.* **2019**, *151*, 060901.
(25) Kershaw, S. V.; Yiu, W. K.; Sergeev, A.; Rogach, A. L. Development of Synthetic Methods to Grow Long-Wavelength Infrared-Emitting HgTe Quantum Dots in Dimethylformamide. *Chem. Mater.* **2020**, *32*, 3930–3943.
(26) Keuleyan, S.; Lhuillier, E.; Guyot-Sionnest, P. Synthesis of Colloidal HgTe Quantum Dots for Narrow Mid-IR Emission and Detection. *J. Am. Chem. Soc.* **2011**, *133*, 16422–16424.
(27) Cryer, M. E.; Fiedler, H.; Halpert, J. E. Photo-Electrosensitive Memristor Using Oxygen Doping in HgTe Nanocrystal Films. *ACS Appl. Mater. Interfaces* **2018**, *10*, 18927–18934.
(28) Lhuillier, E.; Keuleyan, S.; Zolotavin, P.; Guyot-Sionnest, P. Mid-Infrared HgTe/As_2S_3 Field Effect Transistors and Photodetectors. *Adv. Mater.* **2013**, *25*, 137–141.
(29) Liu, H.; Lhuillier, E.; Guyot-Sionnest, P. *1/f* Noise in Semiconductor and Metal Nanocrystal Solids. *J. Appl. Phys.* **2014**, *115*, 154309.
(30) Shen, G.; Chen, M.; Guyot-Sionnest, P. Synthesis of Nonaggregating HgTe Colloidal Quantum Dots and the Emergence of Air-Stable n-Doping. *J. Phys. Chem. Lett.* **2017**, *8*, 2224–2228.
(31) Prado, Y.; Qu, J.; Gréboval, C.; Dabard, C.; Rastogi, P.; Chu, A.; Khalili, A.; Xu, X. Z.; Delerue, C.; Ithurria, S.; et al. Seeded Growth of HgTe Nanocrystals for Shape Control and Their Use in Narrow Infrared Electroluminescence. *Chem. Mater.* **2021**, *33*, 2054–2061.
(32) Chen, M.; Lan, X.; Tang, X.; Wang, Y.; Hudson, M. H.; Talapin, D. V.; Guyot-Sionnest, P. High Carrier Mobility in HgTe Quantum Dot Solids Improves Mid-IR Photodetectors. *ACS Photonics* **2019**, *6*, 2358–2365.
(33) Lan, X.; Chen, M.; Hudson, M. H.; Kamysbayev, V.; Wang, Y.; Guyot-Sionnest, P.; Talapin, D. V. Quantum Dot Solids Showing State-Resolved Band-like Transport. *Nat. Mater.* **2020**, *19*, 323–329.
(34) Zhang, H.; Guyot-Sionnest, P. Shape-Controlled HgTe Colloidal Quantum Dots and Reduced Spin–Orbit Splitting in the Tetrahedral Shape. *J. Phys. Chem. Lett.* **2020**, *11*, 6860–6866.

(35) Mišeikis, V.; Marconi, S.; Giambra, M. A.; Montanaro, A.; Martini, L.; Fabbri, F.; Pezzini, S.; Piccinini, G.; Forti, S.; Terrés, B.; et al. Ultrafast, Zero-Bias, Graphene Photodetectors with Polymeric Gate Dielectric on Passive Photonic Waveguides. *ACS Nano* **2020**, *14*, 11190–11204.
(36) Frisenda, R.; J. Molina-Mendoza, A.; Mueller, T.; Castellanos-Gomez, A.; Zant, H. S. J. van der. Atomically Thin p–n Junctions Based on Two-Dimensional Materials. *Chem. Soc. Rev.* **2018**, *47*, 3339–3358.
(37) Schuler, S.; Schall, D.; Neumaier, D.; Dobusch, L.; Bethge, O.; Schwarz, B.; Krall, M.; Mueller, T. Controlled Generation of a p–n Junction in a Waveguide Integrated Graphene Photodetector. *Nano Lett.* **2016**, *16*, 7107–7112.
(38) Pospischil, A.; Furchi, M. M.; Mueller, T. Solar-Energy Conversion and Light Emission in an Atomic Monolayer p–n Diode. *Nat. Nanotechnol.* **2014**, *9*, 257–261.
(39) Groenendijk, D. J.; Buscema, M.; Steele, G. A.; Michaelis de Vasconcellos, S.; Bratschitsch, R.; van der Zant, H. S. J.; Castellanos-Gomez, A. Photovoltaic and Photothermoelectric Effect in a Double-Gated WSe_2 Device. *Nano Lett.* **2014**, *14*, 5846–5852.
(40) Molina-Mendoza, A. J.; Paur, M.; Mueller, T. Nonvolatile Programmable WSe_2 Photodetector. *Adv. Opt. Mater.* **2020**, *8*, 2000417.
(41) Keuleyan, S. E.; Guyot-Sionnest, P.; Delerue, C.; Allan, G. Mercury Telluride Colloidal Quantum Dots: Electronic Structure, Size-Dependent Spectra, and Photocurrent Detection up to 12 µm. *ACS Nano* **2014**, *8*, 8676–8682.
(42) Allan, G.; Delerue, C. Tight-Binding Calculations of the Optical Properties of HgTe Nanocrystals. *Phys. Rev. B* **2012**, *86*, 165437.
(43) Hudson, M. H.; Chen, M.; Kamysbayev, V.; Janke, E. M.; Lan, X.; Allan, G.; Delerue, C.; Lee, B.; Guyot-Sionnest, P.; Talapin, D. V. Conduction Band Fine Structure in Colloidal HgTe Quantum Dots. *ACS Nano* **2018**, *12*, 9397–9404.
(44) Moghaddam, N.; Gréboval, C.; Qu, J.; Chu, A.; Rastogi, P.; Livache, C.; Khalili, A.; Xu, X. Z.; Baptiste, B.; Klotz, S.; et al. The Strong Confinement Regime in HgTe Two-Dimensional Nanoplatelets. *J. Phys. Chem. C* **2020**, *124*, 23460–23468.
(45) Liu, H.; Keuleyan, S.; Guyot-Sionnest, P. n- and p-Type HgTe Quantum Dot Films. *J. Phys. Chem. C* **2012**, *116*, 1344–1349.
(46) Livache, C.; Izquierdo, E.; Martinez, B.; Dufour, M.; Pierucci, D.; Keuleyan, S.; Cruguel, H.; Becerra, L.; Fave, J. L.; Aubin, H.; et al. Charge Dynamics and Optolectronic Properties in HgTe Colloidal Quantum Wells. *Nano Lett.* **2017**, *17*, 4067–4074.
(47) Noumbé, U. N.; Gréboval, C.; Livache, C.; Chu, A.; Majjad, H.; Parra López, L. E.; Mouafo, L. D. N.; Doudin, B.; Berciaud, S.; Chaste, J.; et al. Reconfigurable 2D/0D *p–n* Graphene/HgTe Nanocrystal Heterostructure for Infrared Detection. *ACS Nano* **2020**, *14*, 4567–4576.
(48) Ackerman, M. M.; Chen, M.; Guyot-Sionnest, P. HgTe Colloidal Quantum Dot Photodiodes for Extended Short-Wave Infrared Detection. *Appl. Phys. Lett.* **2020**, *116*, 083502.
(49) Guyot-Sionnest, P. Electrical Transport in Colloidal Quantum Dot Films. *J. Phys. Chem. Lett.* **2012**, *3*, 1169–1175.
(50) Chuang, C.-H. M.; Maurano, A.; Brandt, R. E.; Hwang, G. W.; Jean, J.; Buonassisi, T.; Bulović, V.; Bawendi, M. G. Open-Circuit Voltage Deficit, Radiative Sub-Bandgap States, and Prospects in Quantum Dot Solar Cells. *Nano Lett.* **2015**, *15*, 3286–3294.
(51) Chen, M.; Shen, G.; Guyot-Sionnest, P. Size Distribution Effects on Mobility and Intraband Gap of HgSe Quantum Dots. *J. Phys. Chem. C* **2020**, *124*, 16216–16221.
(52) Pradhan, S.; Dalmases, M.; Konstantatos, G. Origin of the Below-Bandgap Turn-On Voltage in Light-Emitting Diodes and the High VOC in Solar Cells Comprising Colloidal Quantum Dots with an Engineered Density of States. *J. Phys. Chem. Lett.* **2019**, *10*, 3029–3034.
(53) Sun, B.; Ouellette, O.; García de Arquer, F. P.; Voznyy, O.; Kim, Y.; Wei, M.; Proppe, A. H.; Saidaminov, M. I.; Xu, J.; Liu, M.; et al. Multibandgap Quantum Dot Ensembles for Solar-Matched Infrared Energy Harvesting. *Nat. Commun.* **2018**, *9*, 4003.
(54) Gréboval, C.; Chu, A.; Goubet, N.; Livache, C.; Ithurria, S.; Lhuillier, E. Mercury Chalcogenide Quantum Dots: Material Perspective for Device Integration. *Chem. Rev.* **2021,** 121, 3627-3700.

TOC graphic